2013 IEEE International Conference on Robotics and Automation (ICRA)
Karlsruhe, Germany, May 6-10, 2013

Vertical vibration suppression for a position controlled biped robot*

Shuuji Kajita[1], Futoshi Asano[1], Mitsuharu Moriswa[1], Kanako Miura[1],
Kenji Kaneko[1], Fumio Kanehiro[1] and Kazuhito Yokoi[1]

***Abstract*— A controller design to suppress vertical vibration of a position controlled biped walking robot is presented. The system model of structural vibration is estimated from a measurement of frequency response. By using the model, an optimal feedback controller with full state observer is designed. With a consideration of leg support phase, the vibration controller is combined into our walking controller. The effectiveness of our controller is experimentally demonstrated.**

I. INTRODUCTION

Vertical vibration causes many problems for biped walking robots. It can lose walking stability by the fluctuation of the floor reaction force. A severe vibration can even damage the robot hardware. Although it was not explicitly mentioned in our former reports [1], [2], vertical vibration has been restricted maximum speed and stride of our walking robots.

It is difficult to control vibration of a walking robot because it does not have a single reason. A robot vibrates because of deformation of the links, compliance of the harmonic gears, joint servo stiffness or loosely attached electronic components. Some of them can be explicitly modeled but most of them are hardly modeled and simulated.

In this paper, we estimate the dynamics of vertical vibration from an experiment taking frequency response of real hardware. The system identification and controller design is done by commercially available software following a standard methodology of modern control theory. By combining the resulted controller to our walking controller, satisfying vibration suppression was obtained.

II. RELATED WORKS

Kim and Oh developed an effective stabilizer for their humanoid robot KHR-1 walking on flat, non-inclined surfaces using an ankle torque feedback to regulate the structural vibration [3]. To let the humanoid robot KHR-2 walk on uneven and inclined floor, Kim, Park and Oh developed more advanced controller consists of six components [4]. Later, it was expanded to handle a large biped robot which can carry a payload over 100 kg [5]. They designed a controller by modeling the structural vibration as a pendulum with a compliant joint. To reduce the landing impact, a virtual shock absorber was implemented. However, this part was designed without an explicit modeling of the the structural vibration dynamics.

Buschmann implemented an online hybrid position/force controller for the walking control of the humanoid robot LOLA developed at Technical University of Munich [6], [7]. His hybrid controller was designed based on a rigid body dynamics and can realize maximum walking speed of 3.34 km/h. However, his success partially owes on the LOLA's superior design which minimizes its mechanical deformation.

For torque controlled walking robots, vertical vibration is not a big problem, because they can generate desired floor reaction force with an appropriate force distribution algorithm [8], [9]. On the other hand, implementing torque controllers for all joints requires higher cost and development time.

III. SYSTEM IDENTIFICATION

A. Frequency response

We consider a humanoid robot HRP-4C, as a typical example which suffers from structural vibration (Fig.1(a)). It is a biped humanoid robot, whose height is 160 cm, weighs 48 kg and has 44 degrees of freedom [10]. To realize similar appearance of average Japanese young female, HRP-4C was designed to have thin link structure. This causes structural vibration which was not prominent in our preceding humanoid robots like HRP-2 [11].

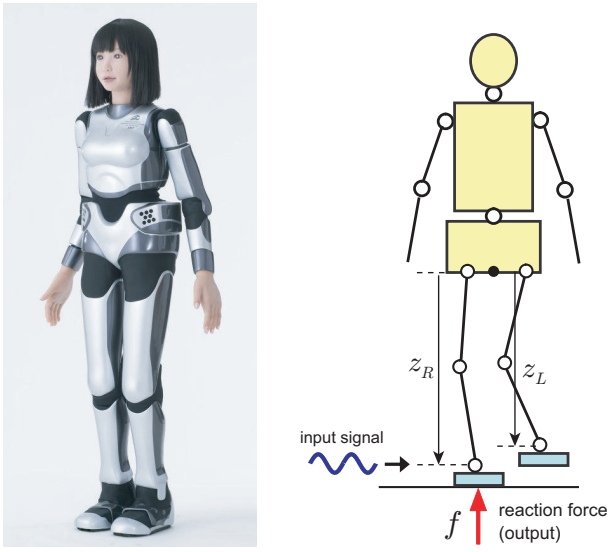

(a) Biped robot HRP-4C (b) Setup for vibration measurement

Fig. 1. The robot and experiment

Figure 1(b) illustrates the way of taking frequency response of our robot. After starting PID servo controllers of

*This work was supported by JST, CREST

[1]S.Kajita, F.Asano, M.Morisawa, K.Miura, K.Kaneko, F.Kanehiro and K.Yokoi are with Intelligent Systems Research Institute, AIST, 1-1-1 Umezono, Tsukuba, Ibaraki, Japan s.kajita at aist.go.jp

all joints of HRP-4C, we have let HRP-4C to stand with one leg. Then we added a small vibration to the supporting foot.

The overridden signal for k-th sampling time is as follows.

$$u_k = A \sin \omega k \Delta t \quad (1)$$
$$v_k = A \cos \omega k \Delta t. \quad (2)$$

In our experiment, $\Delta t = 5$ms. The reference position of the supporting foot was overridden by u_k and converted into the reference joint angles by inverse kinematics. Since it generated the vertical foot motion with respect to the waist link, it excited the oscillation of the whole robot. As the output, we took vertical floor reaction force measured by the sensor in the supporting ankle. We also generated cosine signal (2) to use latter signal processing.

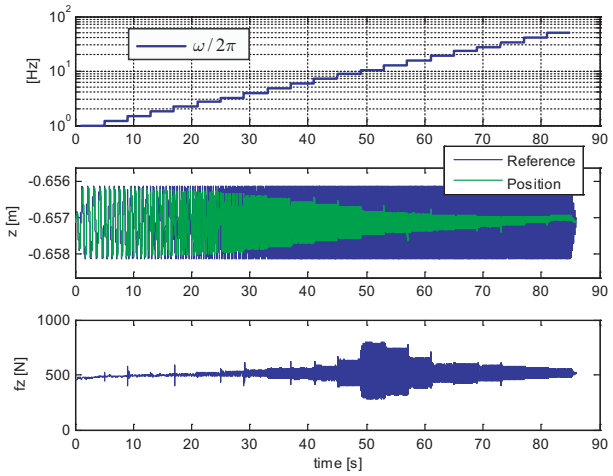

Fig. 2. Vertical excitation experiment

The amplitude A was set to be 1 mm, and the frequency was changed from 1 to 50 Hz with a specified interval period as shown in the upper graph of Fig.2. The foot height with respect to the waist is plotted in the middle graph. The reference and the actual displacement are shown by blue and green lines, respectively. We can observe the actual amplitude gradually get smaller at higher frequency because of the degeneration of the servo tracking.

The bottom graph shows the measured vertical force which has maximum magnitude at about 10 Hz. Using acquired data and the recorded input signals, we calculated Fourier coefficients of discrete time domain for each period of frequency ω. Let us denote the force data at k-th sampling time as f_k.

$$S_\omega = 2 \sum_{k=0}^{N-1} (f_{k+K_\omega} - \bar{f}_\omega) u_k / A \quad (3)$$
$$C_\omega = 2 \sum_{k=0}^{N-1} (f_{k+K_\omega} - \bar{f}_\omega) v_k / A \quad (4)$$
$$\bar{f}_\omega := \frac{1}{N} \sum_{k=0}^{N-1} f_{k+K_\omega}, \quad (5)$$

where K_ω is the staring point of frequency ω and N is the number of data in the period. The gain and phase, g_ω, ϕ_ω is calculated as follows.

$$g_\omega = \sqrt{S_\omega^2 + C_\omega^2}/A \quad (6)$$
$$\phi_\omega = \mathrm{atan2}(C_\omega, S_\omega). \quad (7)$$

Figure 3 shows the bode diagram from the right foot displacement to the floor reaction force. It also shows the frequency response at left leg standing, bode diagram from the left foot oscillation to the floor reaction force. We can see they have close trends except at very low frequency. The difference was caused by the numerical instability of the gain/phase calculation from the short noisy data with respect to the frequency. In the following sections, we only use the data of right leg support.

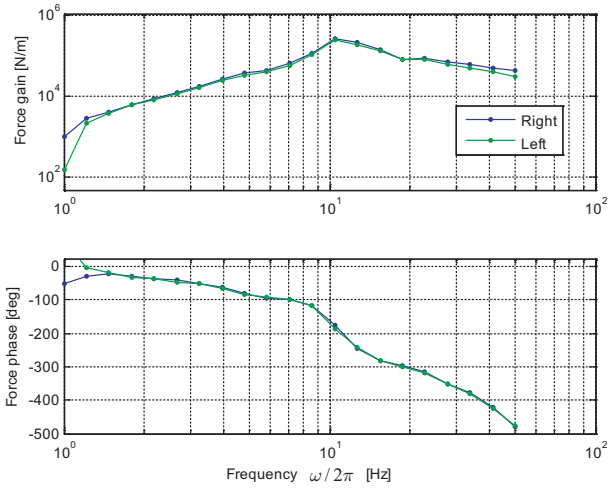

Fig. 3. Bode diagram of force response

B. Frequency response of a mechanical model

At the beginning, we tried to find a mechanical model which can explain the experimental data. For the sake of simplicity, we restricted the model to consist two masses which represent the body and the leg. To reproduce the robot vibration, we assumed springs and dampers which connect these masses and the environment.

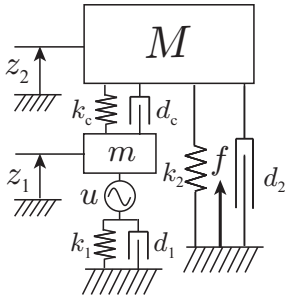

Fig. 4. Two mass model

Figure 4 is an example, which has dynamics of the following equation.

$$\frac{d}{dt}\begin{bmatrix} z_1 \\ \dot{z}_1 \\ z_2 \\ \dot{z}_2 \end{bmatrix} = \boldsymbol{M}\begin{bmatrix} z_1 \\ \dot{z}_1 \\ z_2 \\ \dot{z}_2 \end{bmatrix} + \begin{bmatrix} 0 \\ \frac{k_1}{m} \\ 0 \\ \dot{0} \end{bmatrix} u \qquad (8)$$

$$f = [0\ 0\ -k_2\ -d_2]\begin{bmatrix} z_1 \\ \dot{z}_1 \\ z_2 \\ \dot{z}_2 \end{bmatrix} \qquad (9)$$

$$\boldsymbol{M} := \begin{bmatrix} 0 & 1 & 0 & 0 \\ -\frac{k_c+k_1}{m} & -\frac{d_c+d_1}{m} & \frac{k_c}{m} & \frac{d_c}{m} \\ 0 & 0 & 0 & 1 \\ \frac{k_c}{M} & \frac{d_c}{M} & -\frac{k_c+k_2}{M} & -\frac{d_c+d_2}{M} \end{bmatrix}$$

Figure 5 shows the bode diagram calculated by this model with a certain parameter setting. There exist a lot of possibilities for its parameter tuning as well as the model configuration. We quickly realized that is really difficult to find a good model by this way.

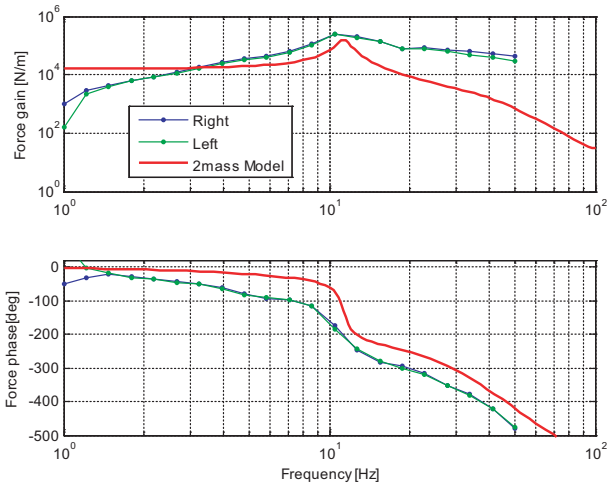

Fig. 5. Bode diagram of a two mass model

C. Model estimation

Instead of assuming a mechanical model, we have decided to estimate a transfer function directly from the frequency response data. There already exist software tools for this purpose, and we used `invfreqz` a Matlab command in Signal Processing Toolbox [12]. This command estimates a discrete-time transfer function corresponding to a given frequency response in the following form.

$$G(z) = \frac{b_n z^n + b_{n-1} z^{n-1} + \ldots + b_0}{a_m z^m + a_{m-1} z^{m-1} + \ldots + a_0}, \qquad (10)$$

where n and m are orders of the numerator and denominator polynomials.

Providing the frequency response data of Fig.**??** and by specifying $n = m = 4$, `invfreqz` command returns a transfer function of

$$G_4(z) = 10^4 \times \frac{-0.629z^4 + 2.26z^3 - 4.92z^2 + 2.87z + 0.540}{z^4 - 2.20z^3 + 2.12z^2 - 1.22z + 0.424}. \qquad (11)$$

Also, by specifying $n = m = 5$, we obtain a transfer function of

$$G_5(z) = 10^4 \times \frac{0.164z^5 - 0.658z^4 + 0.394z^3 - 3.17z^2 + 6.43z - 3.14}{z^5 - 2.50z^4 + 2.53z^3 - 1.45z^2 + 0.643z - 0.161}. \qquad (12)$$

Figure 6 compares the bode diagrams of $G_4(z)$ and $G_5(z)$ with the experimental data. Both of them fit well at the frequency higher than 4 Hz. Although they do not fit well at low frequency, it is not a problem since our main interest is in vibration at high frequency.

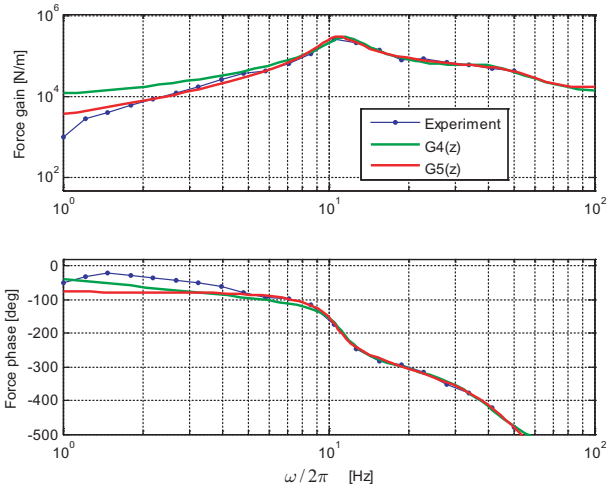

Fig. 6. Frequency response of the estimated model

IV. VIBRATION CONTROLLER DESIGN

The estimated transfer function was converted into the following standard form which is convenient to design a controller.

$$\boldsymbol{x}_{k+1} = \boldsymbol{A}\boldsymbol{x}_k + \boldsymbol{b}u_k \qquad (13)$$

$$f_k = \boldsymbol{c}\boldsymbol{x}_k + du_k \qquad (14)$$

The set of system parameter $(\boldsymbol{A}, \boldsymbol{b}, \boldsymbol{c}, d)$ can be easily obtained from the transfer function $G_4(z)$ or $G_5(z)$. The dimension of the state vector $\boldsymbol{x}$ is four for $G_4(z)$ and five for $G_5(z)$. Unlike the system model in III.B, each element of the state vector $\boldsymbol{x}$ does not hold a simple physical meaning such as position or velocity, because the system dynamics was automatically generated from the frequency response.

A vibration suppression controller can be formed as a state feedback with an observer (Fig.7).

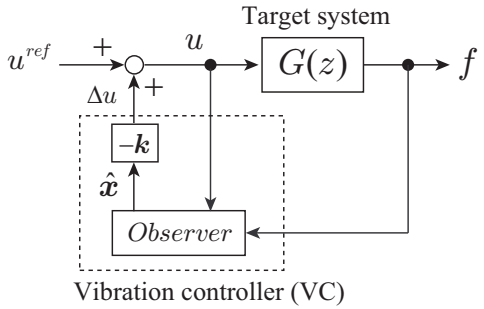

Fig. 7. State feedback by observer

The control low is

$$u_k = u_k^{ref} - \boldsymbol{k}\hat{\boldsymbol{x}}_k, \tag{15}$$

where u_k^{ref} is a reference input and $\boldsymbol{k}$ is a state feedback gain vector. By using Matlab command `dlqr`, we can obtain a feedback gain $\boldsymbol{k}$ to minimize a performance index J of

$$J = \sum_k \{\boldsymbol{x}_k^T \boldsymbol{Q} \boldsymbol{x}_k + R u_k^2\}, \tag{16}$$

where the $n \times n$ matrix $\boldsymbol{Q}$ and the scalar R are parameters to adjust the state feedback gain $\boldsymbol{k}$. Note that these parameters and J do not hold simple physical meaning since the state vector $\boldsymbol{x}$ lacks it as explained at the beginning of this section.

We used a full state observer to calculate an estimated state vector $\hat{\boldsymbol{x}}_k$.

$$\hat{\boldsymbol{x}}_{k+1} = \boldsymbol{A}\hat{\boldsymbol{x}}_k + \boldsymbol{b}u_k - \boldsymbol{l}(\hat{f}_k - f_k), \tag{17}$$

$$\hat{f}_k = \boldsymbol{c}\hat{\boldsymbol{x}}_k + du_k, \tag{18}$$

where $\boldsymbol{l}$ is an observer gain, which can also be calculated by `dlqr` as a least quadratic (LQ) gain for a dual system $(\boldsymbol{A}^T, \boldsymbol{c}^T)$.

Figure 8 is the simulated result using the fourth order model $G_4(z)$ and the proposed controller. In the upper graph, the reference input is plotted by thin green line, and the input modified by state feedback is plotted by bold blue line. In the lower graph, the thin green line is the original oscillatory response without control and the bold blue line is the response under the proposed vibration control. It is seen that the output vibration is effectively suppressed.

Fig. 9 shows the result using the fifth order model $G_5(z)$ in the same manner. We decided to use this controller for our robot, since the peak (bold blue line in the lower graph of Fig. 9) is smaller than in the simulation of forth order model result (bold blue line in the lower graph of Fig. 8).

V. EXPERIMENT

A. Vertical force controller implementation

To evaluate our vibration controller, we conducted a walking experiment using the controller proposed in [1]. Introducing the vibration controller to a biped walking robot requires special consideration. That is not to use the controller for a leg in the air, because it was designed based on an experiment

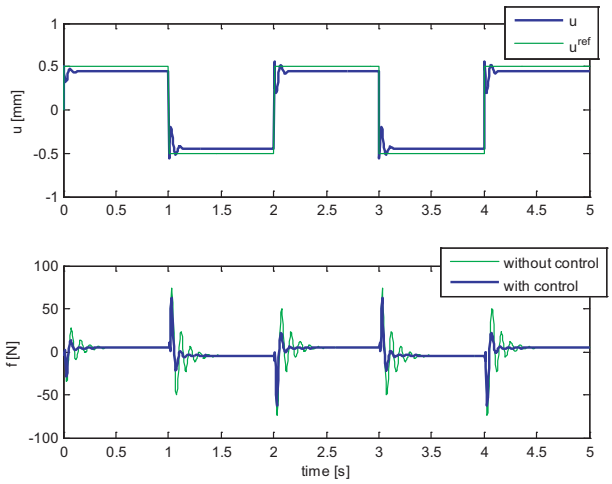

Fig. 8. Vibration control using $G_4(z), \boldsymbol{Q} = \boldsymbol{I}, R = 1 \times 10^8$

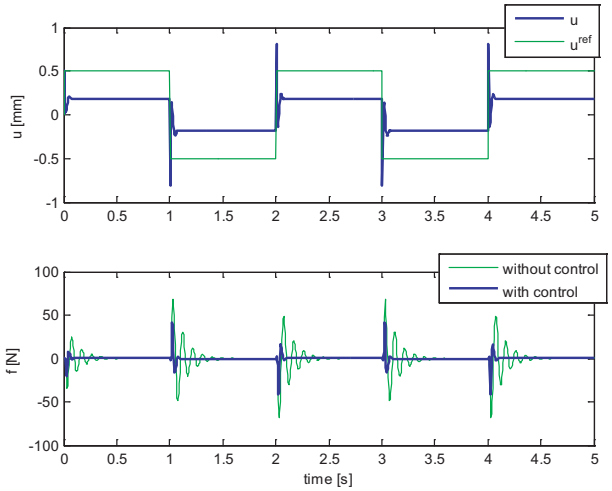

Fig. 9. Vibration control using $G_5(z), \boldsymbol{Q} = \boldsymbol{I}, R = 5 \times 10^8$

of supporting foot on the ground and the controller stability at swing phase is not guaranteed.

For this reason, we modified the vibration controller as following.

$$z_k = z_k^{ref} + \Delta u_k \tag{19}$$

$$\Delta u_k = \begin{cases} -\boldsymbol{k}\hat{\boldsymbol{x}}_k & \text{(if support phase)} \\ (1 - \frac{\Delta t}{T_{zero}})\Delta u_{k-1} & \text{(else)} \end{cases} \tag{20}$$

$$\hat{\boldsymbol{x}}_{k+1} = \begin{cases} \boldsymbol{A}\hat{\boldsymbol{x}}_k + \boldsymbol{b}u_k - \boldsymbol{l}(\hat{f}_k - f_k), & \text{(if support phase)} \\ \boldsymbol{0} & \text{(else)} \end{cases} \tag{21}$$

The vibration controller is only applied when the foot is on the ground, where the floor reaction force exceeds the threshold level. If the foot is in the air, the controller output Δu_k decays by a time constant of T_{zero}. Also, the observer estimates when the foot is in support phase and is reset when the foot is in the air.

The entire structure of our vertical force controller is shown in Fig.10. The inputs for the vibration controllers are

given as

$$z_R^{ref} = z_R^{pg} + 0.5 z^{df} \quad (22)$$
$$z_L^{ref} = z_L^{pg} - 0.5 z^{df}. \quad (23)$$
$$(24)$$

It modifies the foot position commands z_R^{pg}, z_L^{pg} of a walking pattern generator by a damping controller output z^{df} to keep the force difference as the specified value. The damping controller is required to control Zero-Moment Point at double support phase [1], [13] and it is given as follows.

$$z_k^{df} = \begin{cases} z_{k-1}^{df} + \frac{\Delta t}{D}(\delta^d - \delta) - \frac{\Delta t}{T} z_{k-1}^{df} & \text{(if double support)} \\ (1 - \frac{\Delta t}{T_{zero}}) z_{k-1}^{df} & \text{(else)} \end{cases} \quad (25)$$

$$\delta := f_{Lz} - f_{Rz} \quad (26)$$
$$\delta^d := f_{Lz}^d - f_{Rz}^d \quad (27)$$

where D is damping gain. T is a time constant to retrieve the neutral point when a robot is at single support phase.

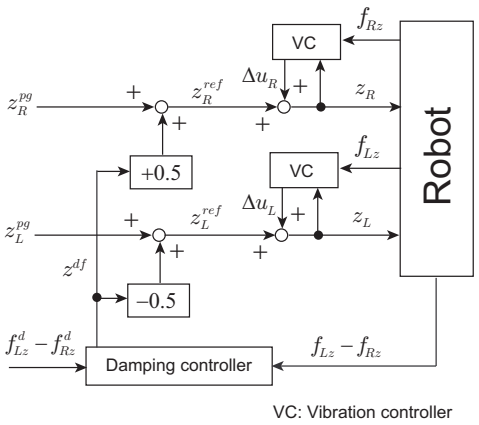

Fig. 10. Control system for floor reaction force

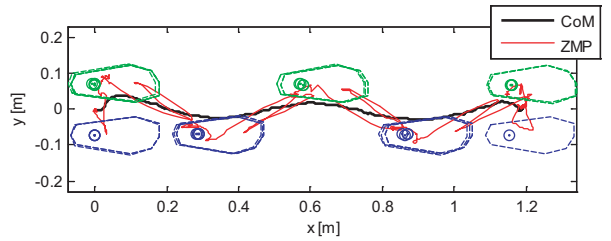

(a) Without vibration supression

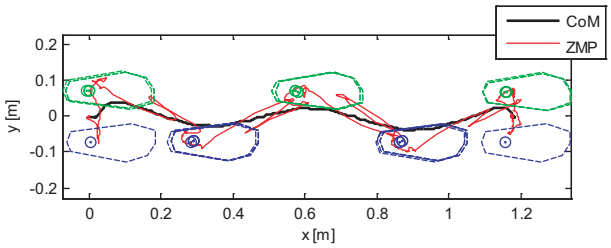

(b) With vibration supression

Fig. 11. Result of the walking experiment

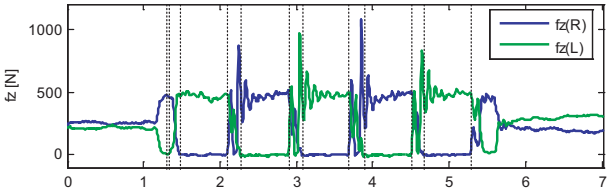

(a) Without vibration control

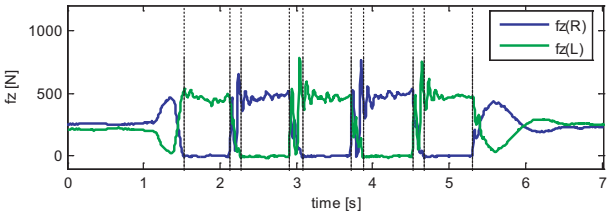

(b) With vibration control

Fig. 12. Vertical floor reaction force

B. Walk experiment

For the walking experiment, we used an offline generated pattern whose step length is 0.3 m and step time is 0.8 s. Figure 11 shows the trajectory of the center of mass (CoM) and Zero-Moment Point (ZMP) during the experiment. In these graphs, we cannot see a big difference between the conventional method and the proposed method.

The effect of the proposed method is clearly seen in the vertical forces plotted in Fig. 12. Without the vibration control, the peak force reaches 1000 N in the middle of walking, which is two times of the robot body weight (Fig.12(a)). With the control, the peaks are drastically reduced. The outputs of vibration controller are shown in the upper graph of Fig.13. Although their magnitude are very small (always less than 3 mm), they quickly change during double support phase of support leg exchange, so that it can suppress the structural vibration of the robot.

Figure 14 shows the vertical acceleration in the same experiment. By using our vibration controller the vertical acceleration at support exchange is reduced. Although our controller only used the vertical force signal, it also reduced the lateral vibration as shown in Fig.15.

VI. CONCLUSIONS AND FUTURE WORK

We explained a systematic method to design a controller to suppress vibration at walking. The same strategy is applicable to another part of walking control. For example, posture stabilization can be a next target, which requires improvement for higher walking performance.

ACKNOWLEDGMENT

We thank members of humanoid robotics group, Dr. Nakaoka, Dr. Kita and Dr. Asoh for their technical help and the fruitful discussion with them. We also thank Mr.Ishiwata

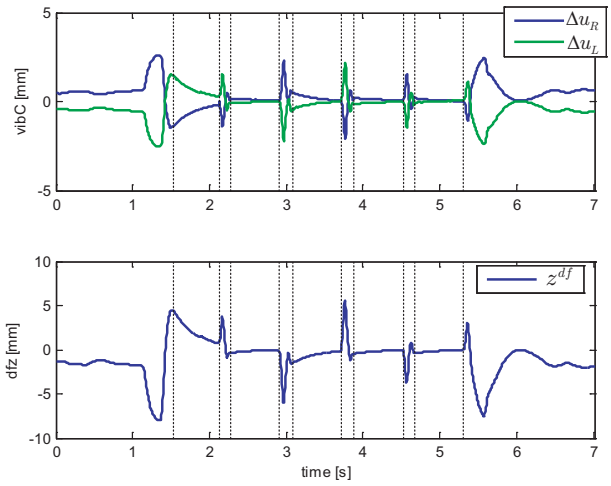

Fig. 13. Controller outputs with vibration control

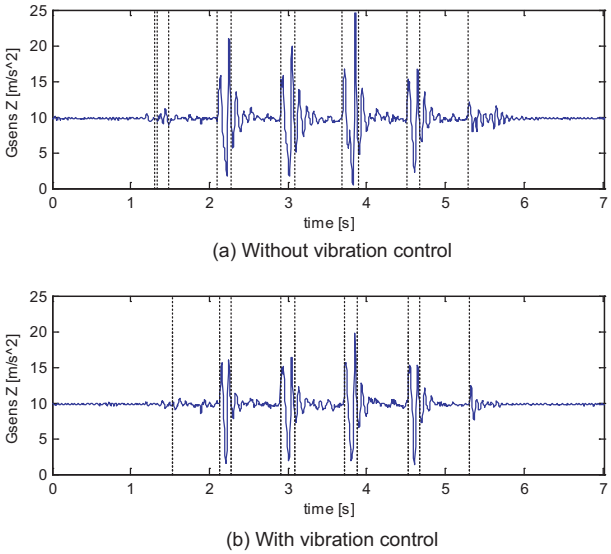

Fig. 14. Body accelerometer (vertical component)

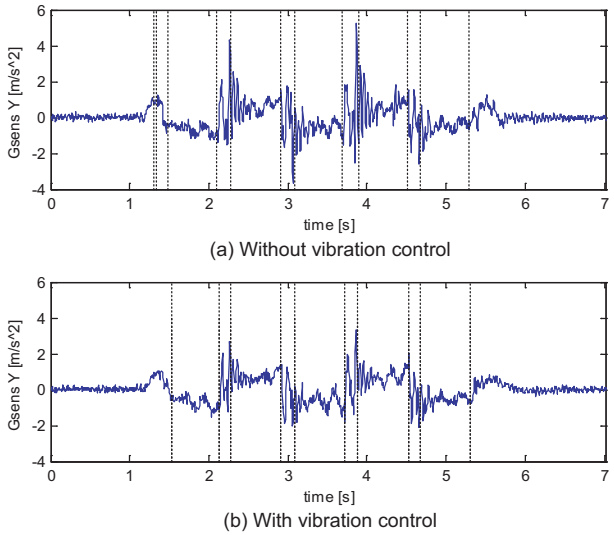

Fig. 15. Body accelerometer (lateral component)

who developed ART-Linux 2.6, a dependable real-time operating system.

REFERENCES

[1] S. Kajita, M. Morisawa et al., "Biped Walking Stabilization Based on Linear Inverted Pendulum Tracking," Inter. Conf. on Intelligent Robots and Systems, pp.4489-4496, 2010.

[2] K. Miura, M. Morisawa et al., "Human-like Walking with Toe Supporting for Humanoids," Inter. Conf. on Intelligent Robots and Systems, pp.4428-4435, 2011.

[3] Jung-Hoon Kim and Jun-Ho Oh, "Walking Control of the Humanoid Platform KHR-1 based on Torque Feedback Control," Proc. of the 2004 IEEE Int. Conference on Robotics and Automation, pp.623-628, 2004.

[4] Jung-Yup Kim, Ill-Woo Park, and Jun-Ho Oh, "Walking Control Algorithm of Biped Humanoid Robot on Uneven and Inclined Floor," Journal of Intelligent and Robotic Systems, Vol. 48, No. 4, pp. 457 - 484, April, 2007.

[5] Jung-Yup Kim, Jungho Lee and Jun-Ho Oh, "Experimental realization of dynamic walking for a human-riding biped robot, HUBO FX-1," Advanced Robotics, vol.21, no.3-4, pp461-484, 2007.

[6] Thomas Buschmann, "Simulation and Control of Biped Walking Robots," Ph.D thesis at Technischen Universität München, 2010.

[7] T. Buschmann, S. Lohmeier and H. Ulbrich, "Biped Walking Control Based on Hybrid Position/Force Control," Proc. of the 2009 IEEE/RSJ Inter. Conf. on Intelligent Robots and Systems, pp.3019-3024, 2009.

[8] S.-H. Hyon, "Compliant terrain adaptation for biped humanoids without measuring ground surface and contact forces," IEEE Trans. Robotics, vol. 25, no.1, 2009.

[9] C. Ott, M. A. Roa, and G. Hirzinger, ' 'Posture and balance control for biped robots based on contact force optimization," Proc. of 2011 Inter. conf. on humanoid robots, pp.26-33, 2011.

[10] K.Kaneko, F.Kanehiro et al., "Hardware Improvement of Cybernetic Human HRP-4C for Entertainment Use," Proc. of IEEE/RSJ Int. Conference on Intelligent Robots and Systems, pp.4392-4399, 2011.

[11] K.Kaneko, F.Kanehiro, S.Kajita, H.Hirukawa et al., "Humanoid Robot HRP-2," Proc. of the 2004 IEEE Int. Conference on Robotics and Automation, pp.1083-1090, 2004.

[12] MathWorks Documentation Center
`http://www.mathworks.com`

[13] M.Vukobratović and B.Borovac, "Zero-Moment Point – Thirty File Years of Its Life –," International Journal of Humanoid Robotics, vol.1, no.1, pp.157-173, 2004.